Molecular Therapy

Original Article



Dibenzazepine-Loaded Nanoparticles Induce Local Browning of White Adipose Tissue to Counteract Obesity

Chunhui Jiang, 1,2,7 Mario Alberto Cano-Vega, 1,2,7 Feng Yue, 3 Liangju Kuang, 1,2 Naagarajan Narayanan, 1,2 Gozde Uzunalli, 1,2 Madeline P. Merkel, 2,4 Shihuan Kuang, 3 and Meng Deng 1,2,5,6

¹Department of Agricultural and Biological Engineering, Purdue University, West Lafayette, IN 47907, USA; ²Bindley Bioscience Center, Purdue University, West Lafayette, IN 47907, USA; ³Department of Animal Sciences, Purdue University, West Lafayette, IN 47907, USA; ⁴College of Pharmacy, Purdue University, West Lafayette, IN 47907, USA; ⁵School of Materials Engineering, Purdue University, West Lafayette, IN 47907, USA; ⁶Weldon School of Biomedical Engineering, Purdue University, West Lafayette, IN 47907, USA; ⁶Weldon School of Biomedical Engineering, Purdue University, West Lafayette, IN 47907, USA; ⁶Weldon School of Biomedical Engineering, Purdue University, West Lafayette, IN 47907, USA; ⁶Weldon School of Biomedical Engineering, Purdue University, West Lafayette, IN 47907, USA; ⁶Weldon School of Biomedical Engineering, Purdue University, West Lafayette, IN 47907, USA; ⁶Weldon School of Biomedical Engineering, Purdue University, West Lafayette, IN 47907, USA; ⁶Weldon School of Biomedical Engineering, Purdue University, West Lafayette, IN 47907, USA; ⁶Weldon School of Biomedical Engineering, Purdue University, West Lafayette, IN 47907, USA; ⁶Weldon School of Biomedical Engineering, Purdue University, West Lafayette, IN 47907, USA; ⁶Weldon School of Biomedical Engineering, Purdue University, West Lafayette, IN 47907, USA; ⁶Weldon School of Biomedical Engineering, Purdue University, West Lafayette, IN 47907, USA; ⁶Weldon School of Biomedical Engineering, Purdue University, West Lafayette, IN 47907, USA; ⁶Weldon School of Biomedical Engineering, Purdue University, West Lafayette, IN 47907, USA; ⁶Weldon School of Biomedical Engineering, Purdue University, West Lafayette, IN 47907, USA; ⁶Weldon School of Biomedical Engineering, Purdue University, West Lafayette, IN 47907, USA; ⁶Weldon School of Biomedical Engineering, Purdue University, West Lafayette, IN 47907, USA; ⁶Weldon School of Biomedical Engineering, Purdue University, West Lafayette, IN 47907, USA; ⁶Weldon School

Inhibition of Notch signaling via systemic drug administration triggers conversion of white adipocytes into beige adipocytes (browning) and reduces adiposity. However, translation of this discovery into clinical practice is challenged by potential offtarget side effects and lack of control over the location and temporal extent of beige adipocyte biogenesis. Here, we demonstrate an alternative approach to stimulate browning using nanoparticles (NPs) composed of FDA-approved poly(lactide-co-glycolide) that enable sustained local release of a Notch inhibitor (dibenzazepine, DBZ). These DBZ-loaded NPs support rapid cellular internalization and inhibit Notch signaling in adipocytes. Importantly, focal injection of these NPs into the inguinal white adipose tissue depots of diet-induced obese mice results in localized NP retention and browning of adipocytes, consequently improving the glucose homeostasis and attenuating body-weight gain of the treated mice. These findings offer new avenues to develop a potential therapeutic strategy for clinical treatment of obesity and its associated metabolic syndrome.

INTRODUCTION

Obesity and its associated comorbidities, including type 2 diabetes, have posed significant challenges to human health. Obesity is driven by a systemic energy surplus stored as lipids in white adipocytes, causing ectopic and excessive deposition of white adipose tissues (WATs). In order to shift the energy balance for obesity treatment, strategies aiming at decreasing energy intake manifest modest efficacy as well as unpleasant, potentially harmful side effects.^{2,3} In contrast, strategies pointing to energy expenditure have sparked enormous interests, mainly due to the newly discovered brown and beige adipocytes in adult humans. 4-8 Brown adipocytes originate and populate in the unique depot of brown adipose tissue (BAT), while beige adipocytes develop in the WAT in response to the control of environmental temperature or sympathetic nerve innervation. 9-13 Both brown and beige adipocytes are densely packed with mitochondria, which possess the robust uncoupled respiration and thermogenic capacity through the uncoupling protein 1 (Ucp1). 14 Notably,

the activities of beige adipocytes correlate with leanness in humans. ^{15,16} Thus, promoting the transformation of white adipocytes into beige adipocytes holds great promise as a new therapeutic strategy to reduce adiposity and its associated risks of metabolic syndromes.

The Notch signaling pathway is an evolutionarily conserved signaling cascade critical for embryonic development, stem cell fate, and tumorigenesis.¹⁷ We have recently reported that inhibition of Notch signaling through intraperitoneal (i.p.) injection of dibenzazepine (DBZ, a y-secretase inhibitor) results in browning of white adipocytes, reduced obesity, and improved glucose balance in obese mice. 18 As DBZ also improves systemic metabolism through its action in the liver, 19 it remains elusive whether browning of WAT has a direct contribution to the observed metabolic improvements after Notch inhibition. Moreover, translation of this approach for obesity treatment is hindered by the risks of off-target consequences and lack of control over the location and temporal extent of beige adipocyte biogenesis. To circumvent these caveats, it is necessary to develop strategies for direct delivery of Notch inhibitors to specific WAT depots to induce local browning and bypass off-target effects. In addition, sustained inhibition of Notch signaling over an extended period would improve the efficacy of this treatment.

Herein, we report the development of nanoparticles (NPs) for direct intracellular delivery of DBZ to the adipocytes within specific subcutaneous WAT depots based on biodegradable and biocompatible polymers. We chose poly(lactide-co-glycolide) (PLGA) as the delivery

Received 6 March 2017; accepted 31 May 2017; http://dx.doi.org/10.1016/j.ymthe.2017.05.020.

⁷The authors contributed equally to this work.

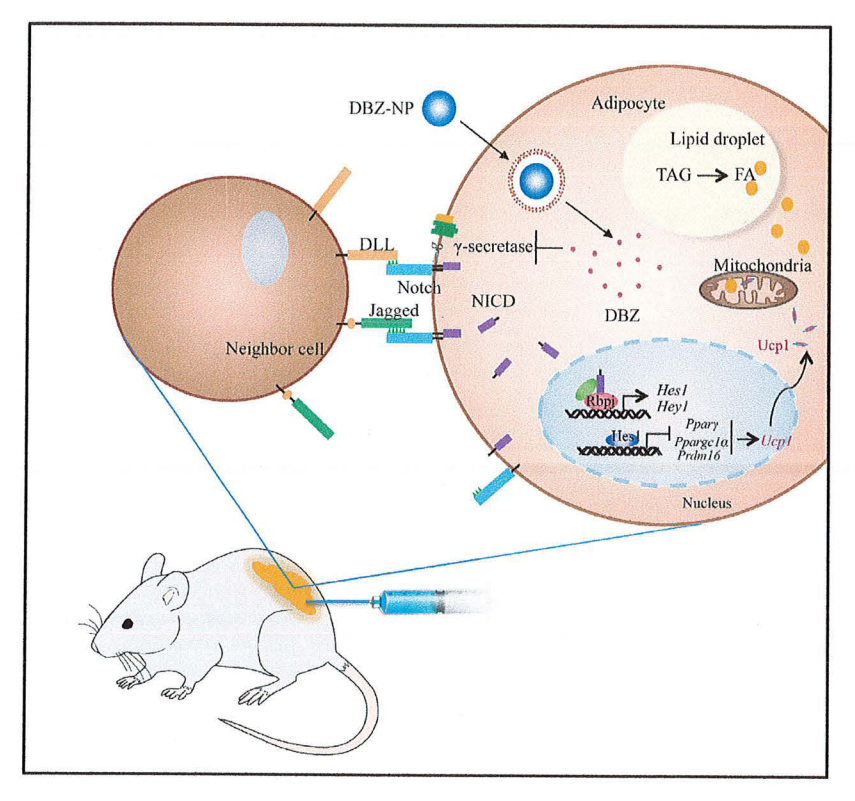
Correspondence: Meng Deng, Department of Agricultural and Biological Engineering, Purdue University, West Lafayette, IN 47907, USA.

E-mail: deng65@purdue.edu

Correspondence: Shihuan Kuang, Department of Animal Sciences, Purdue University, West Lafayette, IN 47907, USA.

E-mail: skuang@purdue.edu





system due to its approval by the Food and Drug Administration (FDA) for a number of clinical applications. As shown in Figure 1, local injection of these DBZ-loaded PLGA NPs (DBZ-NPs) into the inguinal WAT depots results in efficient cellular NP uptake and localized NP retention by the adipocytes. These DBZ-NPs inhibit Notch signaling and promote browning through sustained release of DBZ with predictable release kinetics. These Notch-inhibitor-releasing NPs not only provide mechanistic insights into the direct contribution of the Notch inhibition in the WAT to browning and systemic metabolic improvements, but also offer new avenues to develop a potential therapeutic strategy for the treatment of obesity and its associated metabolic syndrome.

RESULTS

Synthesis and Characterization of NPs

The DBZ-NPs were formulated at a DBZ/PLGA mass ratio of 1:19 using an optimized nanoprecipitation method with an encapsulation efficiency of 94% (Table S1). Transmission electron microscopy (TEM) showed the spherical structures of synthesized DBZ-NPs (Figure 2A). As shown in Figure 2B, the NP size was determined to be 177 ± 6 nm by dynamic light scattering (DLS). Similarly sized bare PLGA-NPs were used as controls. The surface zeta potential for the DBZ-NPs in water was -20.2 ± 3.0 mV.

To evaluate DBZ release characteristics, we investigated in vitro release profiles of DBZ from DBZ-NPs under neutral (1 \times PBS buffer

Figure 1. Schematic Illustration of DBZ-Releasing NPs for Intracellular Induction of Browning through Inhibition of Notch Signaling after Local Injection into Inquinal WAT

Activation of Notch signaling involves binding of DII or Jag family ligands to Notch receptors (Notch1-Notch4), the release of Notch intracellular domain (NICD) via γ-secretase-mediated proteolytic cleavage, and translocation of NICD to the nucleus where it binds Rbpj transcriptional complex and activates the transcription of Hairy/ enhancer-of-split (Hes) and Hes-related with YRPW motif protein (Hey) family genes. Hes1 directly binds to the promoter regions of Prdm16 and Ppargc1a to inhibit the transcription of these two master regulators of mitochondrial biogenesis and beige adipogenesis. As the proteolytic cleavage of NICD is necessary for Notch signaling to occur, pharmacological blockage of this cleavage using NP-based intracellular DBZ delivery provides an effective pathway to inhibit Notch signaling transduction and promote browning. Once taken up by the adipocytes, the NPs release DBZ to locally inhibit Notch signaling over an extended period.

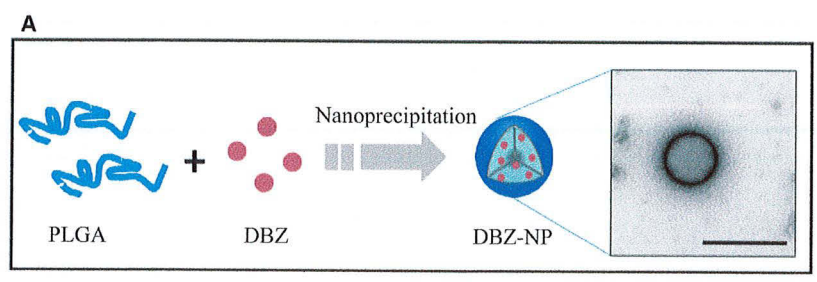
[pH 7.4]) and acidic (1 \times PBS buffer [pH 5.0]) conditions at 37°C. The DBZ-NPs presented continuous release of DBZ, which resulted in 50% of the loaded DBZ to release within 1 day at pH 5.0 and 3 days at pH 7.4, respectively (Figure 2C). In addition, the DBZ release from the

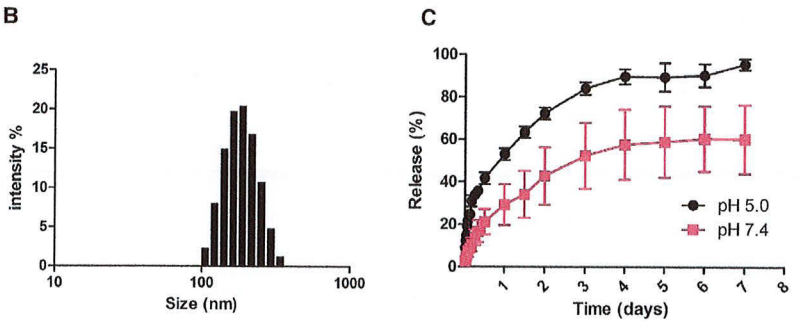
DBZ-NPs was further analyzed using different mathematical models (Table S2). The release data fit well to the Korsmeyer-Peppas model at both pH values (Figure S1), indicating diffusional release of DBZ.

Cellular Uptake of NPs

To confirm the intracellular delivery of the NPs, we examined uptake of NPs by primary preadipocytes using fluorescence microscopy. The stromal vascular fraction (SVF) cells containing preadipocytes were isolated from inguinal WAT and cultured, followed by incubation with NPs encapsulating a Nile red fluorescent dye to facilitate visualization. Within 10 min of incubation, the Nile-red-labeled NPs were taken up by the preadipocytes, and Nile red signals co-localized with late endo/lysosomes (stained with LysoTracker Green [LTG]), indicating a relatively rapid endocytosis of NPs (Figure 3A). When the incubation time was prolonged to 60 min, NPs were distributed throughout the cytoplasm and around the nucleus, suggesting the endolysosomal escape of NPs (Figure 3A).

Next, the endocytosis process of NPs was further visualized by TEM imaging. After 10 min of incubation, NPs were clearly identified in both the endocytic vesicles and the endosomes (Figure 3B), in agreement with the results obtained by fluorescence microscopy. To further validate the cellular uptake of NPs at the tissue level, inguinal WATs were retrieved from mice and subsequently incubated with Nile-red-loaded NPs. After 24 hr of incubation, the red fluorescence was observed throughout a host of mature adipocytes (Figure S2A).





The cellular uptake of NPs was further confirmed by the TEM imaging of inguinal WAT (Figure S2B), demonstrating the localization of NPs within the adipocytes. Our data suggested that the NPs were rapidly internalized by both preadipocytes and mature adipocytes through the endocytotic pathway.

NPs Inhibit Notch Signaling and Promote Browning In Vitro

To test the bioactivity of the DBZ-NPs in suppressing Notch signaling and stimulating browning in vitro, adipogenic differentiation of SVF cells was induced in the presence of DBZ-NPs or control PLGA-NPs. After 8 days of differentiation, we examined the mRNA levels of the Notch targets and the browning markers by qPCR assay. The expression of classical Notch target genes, Hey1, HeyL, and Hes1, was significantly inhibited by the treatment of the DBZ-NPs (Figure 4A). Meanwhile, the mRNA levels of the browning markers, including Ucp1, Cidea, Ppargc1a, and Dio2, were elevated significantly (Figure 4B). The mRNA level of the cytochrome c oxidative subunit 5b (Cox5b) was also increased significantly with the treatment of the DBZ-NPs (by 69%, Figure 4C), confirming that browning is intrinsically associated with the mitochondrial biogenesis and oxidative capacity. Consistently, western blot analysis showed that the protein level of Hes1 was decreased, whereas that of Pgc1- α (encoded by Ppargc1a) was increased markedly (Figures 4D and 4E), suggesting the inhibition of Notch signaling and induction of browning by the DBZ-NPs.

To determine whether these molecular alterations can be correlated with changes in cellular respiration, the oxygen consumption rate (OCR) of the differentiated adipocytes was investigated using an XF24 analyzer. Adipocytes treated with DBZ-NPs exhibited significantly higher OCR under both basal and proton leak conditions (Figure 4F). Collectively, these results suggested that DBZ released from

Figure 2. Nanoparticle Fabrication and Characterization

(A) Schematic illustration of the synthesis of DBZ-NPs by nanoprecipitation at a DBZ/PLGA mass ratio of 1:19. The morphology of DBZ-NPs was characterized by TEM. Scale bar, 200 nm. (B) Size distribution of DBZ-NPs measured by DLS. (C) In vitro release profiles of DBZ from DBZ-NPs at pH 5.0 and 7.4. Data are shown as mean \pm SEM. n = 3 for each group.

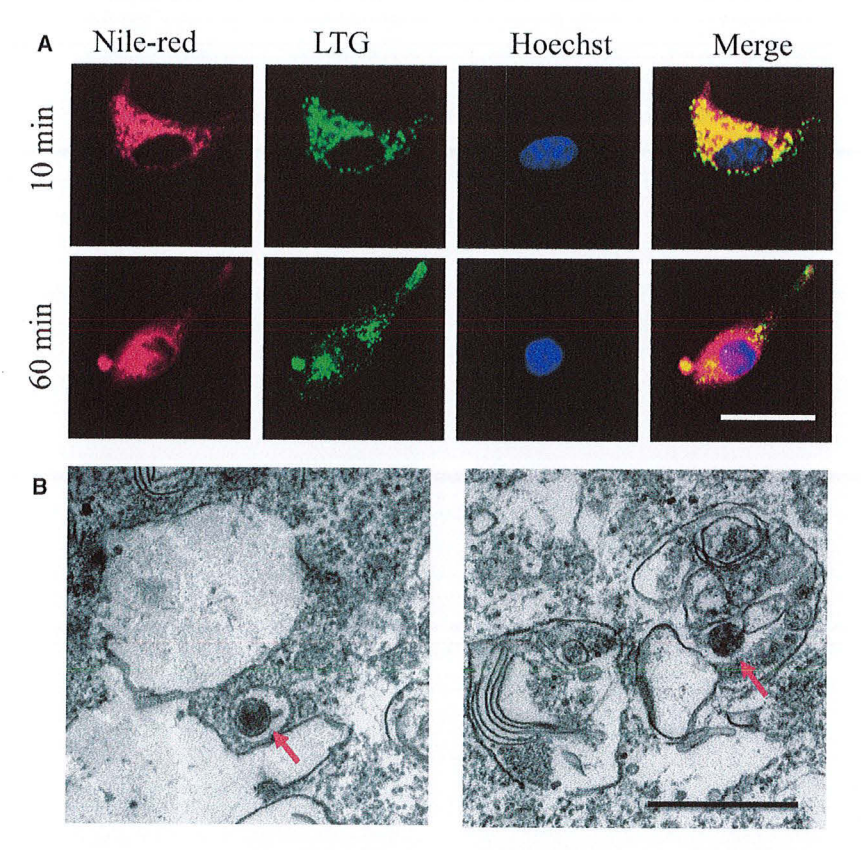
NPs retained its bioactivity to inhibit Notch and thus induce browning of white adipocytes in vitro.

Local Retention and Browning Effects of NPs In Vivo

To assess the performance of NPs in vivo, we first examined the in vivo biodistribution of Cy5.5-labeled PLGA NPs (Cy5.5-NPs) following injection into the inguinal WAT depots using a non-invasive near-infrared optical

imaging technique. The near-infrared fluorescence dye Cy5.5-NHS ester was conjugated to PLGA-NH2 through amide bond formation, followed by the standard formulation of NPs (Figure S3). It was evident from DLS that the average particle sizes of the fabricated Cy5.5-NPs and DBZ-NPs were comparable (Figure S4). The Cy5.5-NPs were then injected into the inguinal WAT depots, which constitute the widely investigated fat tissue due to its significant capability to recruit beige adipocytes.²¹ After 24 hr of administration, Cy5.5-NPs presented an intense fluorescence signal at the injection site (Figure 5A). As time increased, the fluorescence intensity of Cy5.5-NPs decreased with fluorescence signals but retained in the WAT depot until 72 hr post-injection, indicating a robust NP retention within the WAT (Figures 5A and S4). At 72 hr after injection, the mice were immediately euthanized, and various tissues including inguinal WAT, anterior subcutaneous WAT, BAT, muscle, liver, spleen, kidney, and heart were harvested for ex vivo imaging. It is noteworthy that the fluorescence signal of Cy5.5-NPs was exclusively detected in the inguinal WAT while absent in the other off-target tissues (Figure 5B), which was in agreement with the findings from the in vivo fluorescence imaging. In addition, TEM analysis of inguinal WAT further confirmed the localization of NPs within the adipocytes after in vivo injection (Figure 5C). Altogether, the data support the validity of NPs in achieving local delivery to the inguinal WAT depots while minimizing off-target effects.

We next evaluated the efficacy of our DBZ-NPs in inhibiting Notch signaling and promoting browning in vivo. We employed the high-fat diet (HFD)-induced obese mouse model and injected DBZ-NPs to the inguinal WAT depots of mice once per week for 5 weeks. After that, we first confirmed that DBZ-NPs significantly decreased the protein levels of Hes1, indicating the inhibition of Notch activity (Figure S6). Furthermore, total RNA was extracted from inguinal WAT,



followed by the qPCR analysis. As shown in Figure 5D, the mRNA level of *Ucp1* was upregulated 6-fold in the DBZ-NP group as compared to the control PLGA-NP group. Consistently, the mRNA levels of mitochondrial genes *Cox5b* and *Cox7a* were increased dramatically by the DBZ-NPs as compared to the controls (Figure 5E). These molecular changes were corroborated by the H&E and Ucp1 immunohistochemical staining of the inguinal WAT, demonstrating robust browning effects resulting from the DBZ-NP treatment as evidenced from multilocular lipid droplets, shrinkage of adipocytes, and elevated Ucp1 expression (Figure 5F). Thus, local delivery of DBZ-NPs effectively inhibits Notch signaling and induces browning of local WAT in vivo.

NP-Induced Local Browning Improves Metabolism and Prevents Diet-Induced Obesity

We further assessed whether the inductive browning of the local inguinal WAT depots by DBZ-NPs could regulate metabolism and reduce obesity in obese mice. Specifically, we injected DBZ-NPs into the inguinal WAT depots of HFD-induced obese mice once per week to determine the effects of browning induced by DBZ-NPs on body weight, adipocyte tissue morphology, and glucose homeostasis. Notably, the DBZ-NP treatment attenuated the body-weight gain seen in the PLGA-NP-treated control group without affecting energy intake of the mice (Figures 6A and 6B). After 5 weeks

Figure 3. In Vitro Cellular Uptake of NPs

(A) Cellular uptake of Nile-red-labeled NPs in primary preadipocytes within 10 (top) and 60 (bottom) min observed by fluorescence microscopy. Late endo/lysosomes were stained with LysoTracker Green (LTG), and nuclei were stained with Hoechst 33342. Scale bar, 20 μm . (B) Representative TEM images of NPs in the endocytic vesicle (left) and endosome (right). The arrows point to the NPs. Scale bar, 500 nm.

of treatment, mice were euthanized, and tissue samples were retrieved. The inguinal WAT from DBZ-NP-treated mice appeared smaller in size and weighed significantly less as compared to the PLGA-NP counterparts (Figures 6C and 6D). More interestingly, local injection of DBZ-NPs led to significantly enhanced glucose tolerance (Figure 6E) and insulin sensitivity (Figure 6F) as evidenced from intraperitoneal glucose- and insulin-tolerance tests (IP-GTT and IP-ITT, respectively). Consistently, plasma chemistry analysis demonstrated a significant 54% reduction in glucose level in the mice treated with DBZ-NPs as compared to the mice with PLGA-NPs (Figure 6G). Similarly, the blood cholesterol level was 47% lower in the mice receiving DBZ-NPs than that in the control mice (Figure 6H). A similar decreasing trend was

observed in levels of plasma insulin (Figure 6I), triglyceride, free fatty acids, and insulin resistance (Figure S5) in the mice receiving DBZ-NPs, but the differences were not significant. These results together provide encouraging evidence that the induced browning by local delivery of DBZ-NPs to WAT can exert significant and positive metabolic effects in prevention of HFD-induced obesity.

DISCUSSION

Notch signaling plays fundamental roles in regulating cell-cell communication and cell-fate determination during multiple tissue and organ development. For example, it has been reported to influence muscle regeneration, 22,23 bone formation, 24,25 and angiogenesis. 26,27 Nevertheless, the role of Notch in adipogenesis and adipocyte plasticity has just begun to be understood. We have recently discovered that Notch signaling plays an important role in regulating beige adipocyte development in mice. 18 It has been demonstrated that pharmacological inhibition of Notch signaling through the i.p. injection of the Notch inhibitor DBZ promotes widespread browning of WAT. 18 Specifically, this browning phenotype results in increased energy expenditure, enhanced glucose tolerance and insulin sensitivity, and resistance to HFD-induced obesity. However, the direct contribution of browning of white adipocytes to metabolic improvements after Notch inhibition remains to be elucidated. In addition, translating these new findings into the clinic is challenged by the relatively large

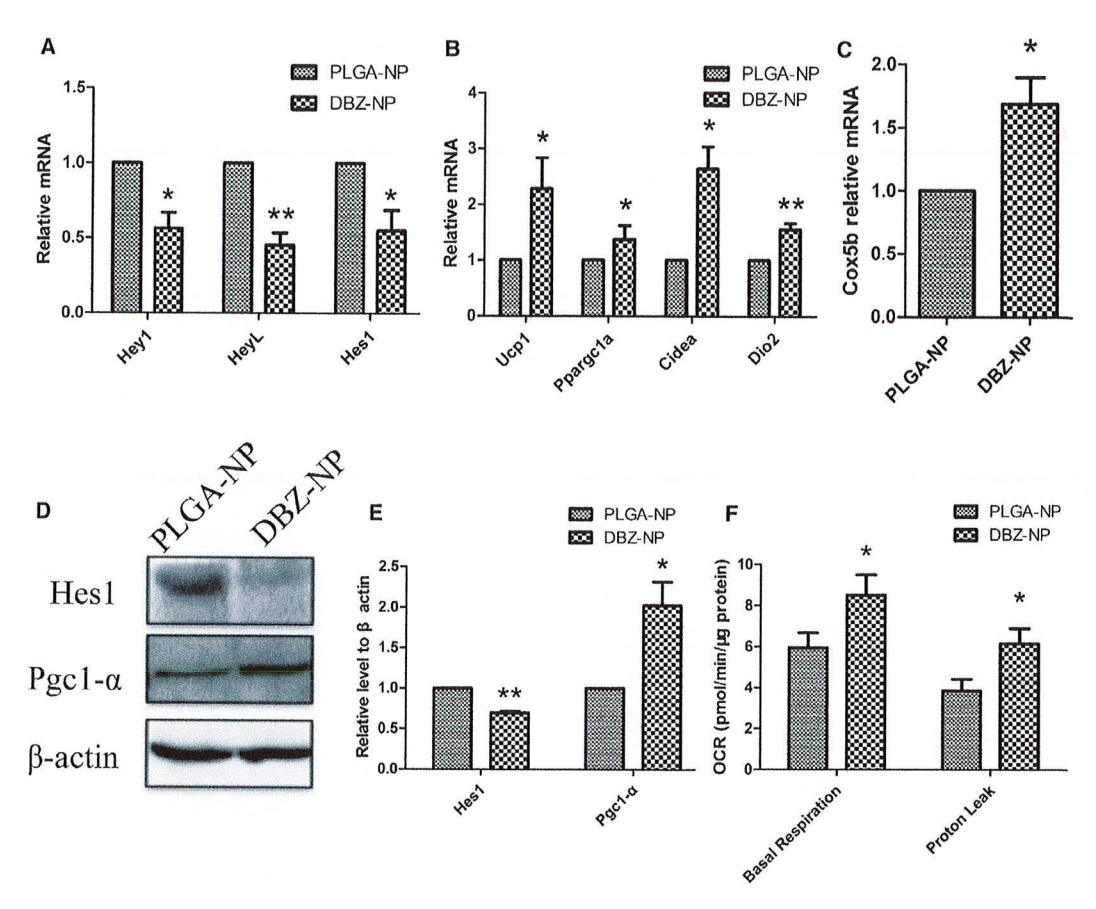


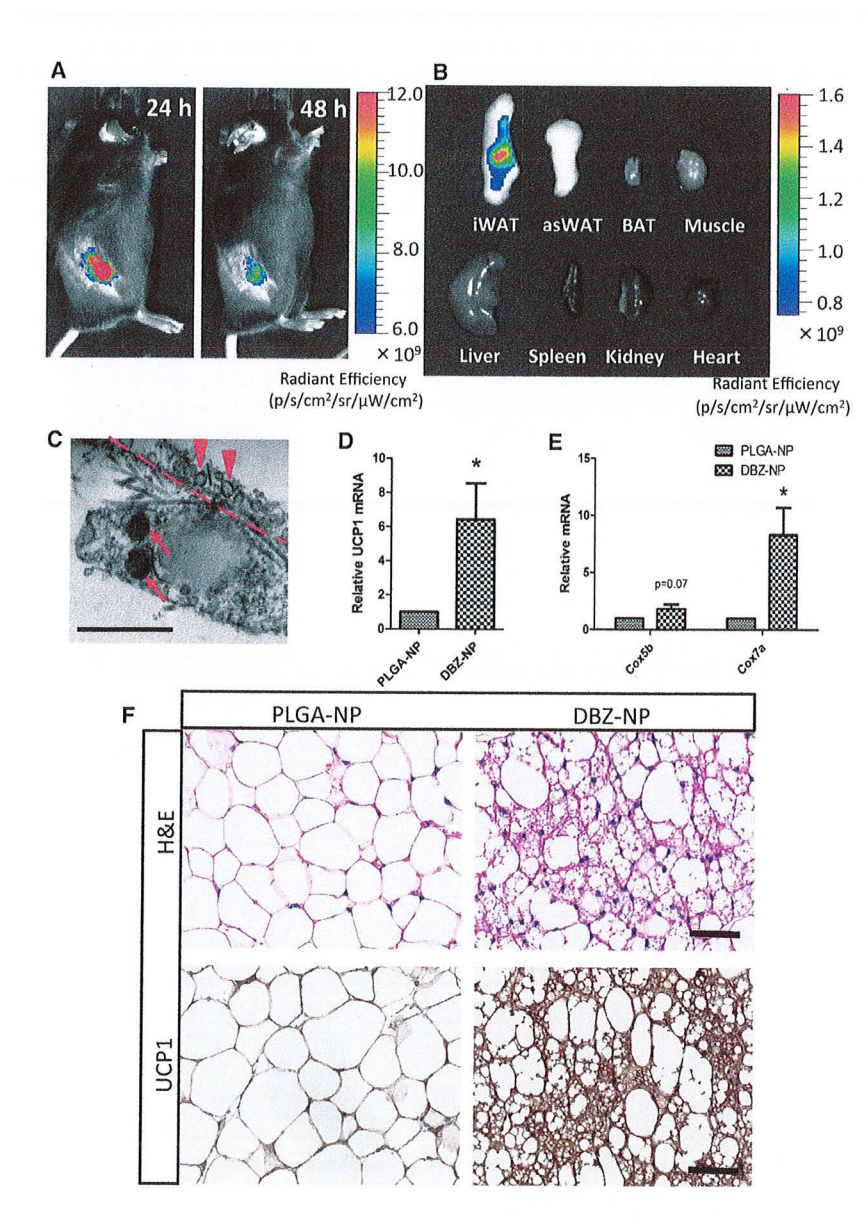
Figure 4. DBZ-NPs Inhibit Notch Signaling and Induce Browning In Vitro (A–C) qPCR analysis showing the mRNA levels of (A) Notch target genes, (B) browning marker genes, and (C) mitochondrial gene Cox5b in differentiated adipocytes treated with PLGA-NPs and DBZ-NPs. (D) Representative western blot results showing the protein expression levels of Hes1 and Pgc-1 α in differentiated adipocytes treated with PLGA-NPs and DBZ-NPs. (E) Quantification of protein levels of Hes1 and Pgc-1 α normalized to β -actin controls by densitometry analysis. (F) OCR under the conditions of basal respiration and proton leak normalized to total protein from differentiated adipocytes. Data are shown as the means \pm SEM. n = 3 batches of SVF cells isolated from three different mice for each group. *p < 0.05, **p < 0.01.

systemic dose requirement, which, in addition to its effect on WAT, may lead to off-target effects of Notch inhibition in other tissues. Here, we demonstrate a controlled, local delivery approach using engineered DBZ-releasing PLGA NPs to selectively induce browning of WAT, improving systemic metabolism and eliciting anti-obesity effects.

We sought to develop a local drug delivery strategy to regulate browning of WAT based on the following rationale: (1) WAT is the primary site of long-term energy storage in most vertebrate species. In response to excess calorie intake, the size of the WAT expands through hyperplasia and hypertrophy of adipocytes. The discovery of beige adipose tissue in WAT depots attests to the promise of modulating massively expanded WAT for obesity treatment. Similar to BAT, beige adipose tissue can produce heat through uncoupling mitochondrial respiration and ATP synthesis via Ucp1. While pro-

ducing heat, beige adipose tissue consumes not only free fatty acid but also large amounts of glucose, thus providing benefits to metabolic health. (2) Local delivery allows a therapeutic concentration of the drug to be delivered directly to the WAT.²⁸ This could circumvent the need to administer a high dose of the drug via conventional systemic drug delivery approaches and minimize off-target side effects. (3) A systemic drug delivery approach may lead to undesired drug accumulation in the liver, an important metabolic organ regulating lipid metabolism, complicating the identification of the working mechanism of Notch signaling, browning of WAT, and systematic metabolic effects.

Engineered drug delivery systems composed of polymeric NPs have shown significant therapeutic efficacy in both basic research and clinical applications. ^{20,29} Polymeric NPs in the size range of 100–300 nm can encapsulate and protect the therapeutics and are particularly



attractive carriers for intracellular drug delivery. ³⁰ Here, a nanoprecipitation method was optimized to produce DBZ-NPs with an average size of 177 nm and high encapsulation efficiency. These NPs can be rapidly internalized by the cells of WAT through endocytotic trafficking and subsequently underwent a rapid endo-lysosome escape to the cytosol, possibly due to the selective reversal from anionic to cationic surface charge in the acidic endo-lysosome compartment. ³¹ This rapid escape also minimizes the burst release of DBZ in the acidic endo-lysosome compartment and allows for prolonged continuous release in the physiological condition, manifested by the differential release profiles of DBZ at pH 5.0 and 7.4. Furthermore, the DBZ released from DBZ-NPs exhibited significant bioactivity as evidenced by the direct inhibition of Notch target genes and the resultant eleva-

Figure 5. The Local Retention of DBZ-NPs Promotes Browning of Inguinal WAT

(A) In vivo fluorescence imaging at 24 and 48 hr after local injection of Cy5.5-NPs into inguinal WAT depot. (B) Ex vivo fluorescence imaging of different tissues at 72 hr post-injection. iWAT, inquinal WAT; asWAT, anterior subcutaneous WAT; BAT, brown adipose tissue. (C) Representative TEM image showing the localization of NPs inside the adipocytes. The arrows point to the NPs. The dotted line and the arrowheads indicate the cell membrane and membrane vesicles, respectively. Scale bar, 500 nm. (D and E) qPCR analysis showing the mRNA levels of (D) Ucp1 and (E) mitochondrial genes, Cox5b and Cox7a from mice treated with PLGA-NPs and DBZ-NPs. Data are shown as the means + SFM, n = 7 mice for each group. *p < 0.05. (F) Representative images of H&E and Ucp1 staining of inguinal WAT after treatment with PLGA-NPs and DBZ-NPs. Scale bar, 50 µm.

tion of browning marker and mitochondrial genes. These results are consistent with our earlier observations from DBZ-loaded microspheres, which cannot be internalized into adipocytes due to their large sizes. The NP-mediated delivery offers unique advantages in enhancing the therapeutic efficacy and minimizing potential side effects by leveraging cellular internalization and intracellular drug release. Notably, it was suggested from controlled-release data that the NPs could efficiently cause Notch inhibition at a dosage 50 times lower than that required for i.p. injection and ten times lower than that needed for microsphere-mediated delivery. The NPs could efficiently cause Notch inhibition at a dosage for times lower than that needed for microsphere-mediated delivery.

Through direct injection of NPs into inguinal WAT, we noted that the NPs were highly concentrated in the local depots, which is highly desirable to mitigate the undesired off-target effects on other tissues. This remarkable local retention could likely be attributed to a combi-

nation of rapid cellular uptake and relatively low density of vasculature in WAT, which minimizes the circulation of NPs. Importantly, we have demonstrated that the local delivery of DBZ-NPs induced browning, prevented HFD-induced obesity and improved glucose homeostasis, verifying the direct regulatory effects of Notch inhibition in WAT on the systemic metabolic profiles.³² These systemic benefits elicited by the local regulation of WAT are in agreement with the recent literature findings that the transplantation of either subcutaneous WAT from exercise-trained mice or BAT from normal mice significantly improved glucose tolerance and insulin sensitivity.^{33,34} It remains to be determined whether these metabolic benefits are solely due to the elevated uptake of glucose and fatty acids or additionally involve other endocrine factors secreted by the transformed

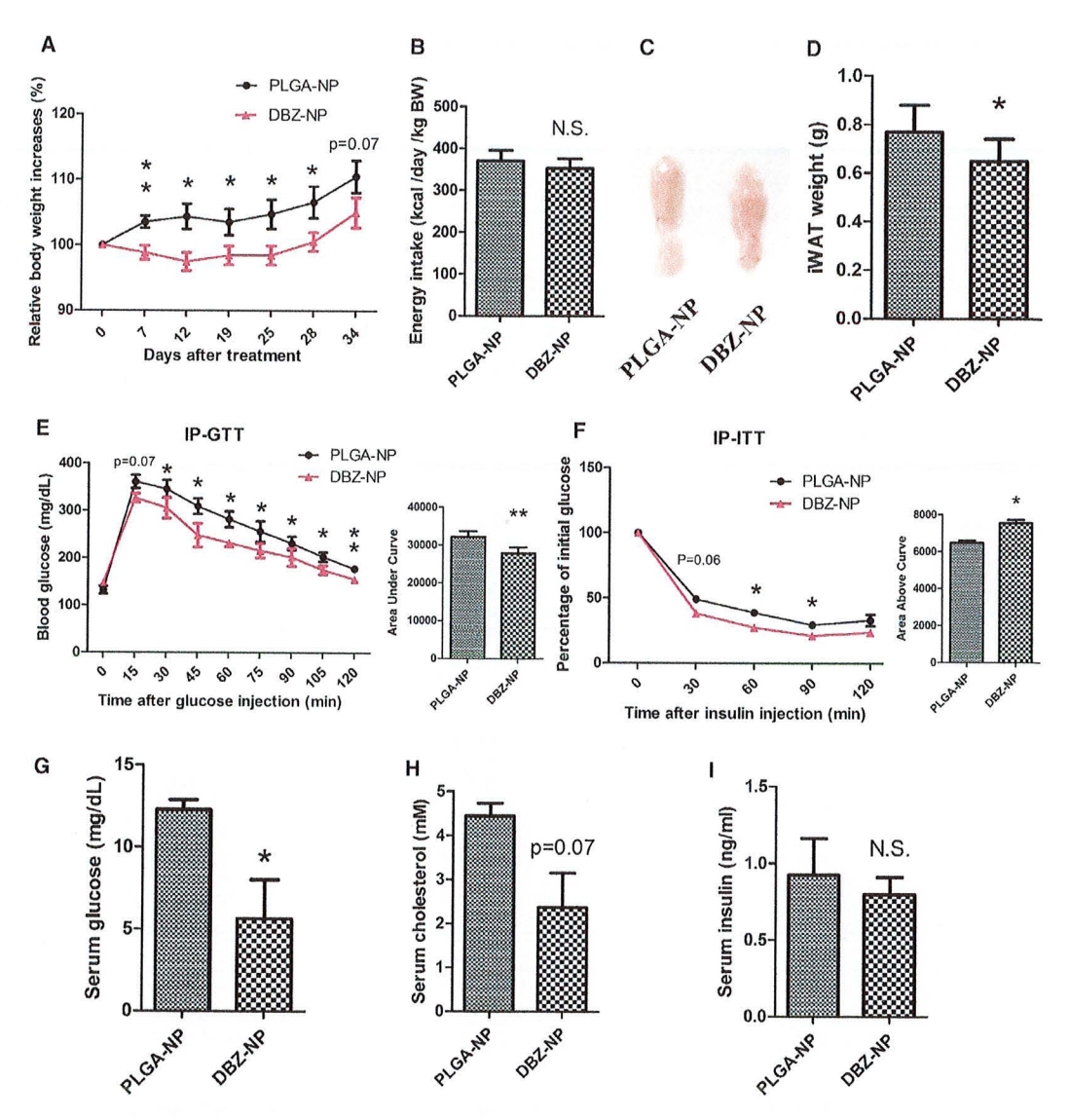


Figure 6. DBZ-NPs Prevent HFD-Induced Obesity

(A) Relative body-weight increases of mice receiving PLGA-NPs and DBZ-NPs after normalization to initial body weight. (B) Average energy intake per mouse per day after normalization to body weight. (C) Representative images of inguinal WAT after treatment with PLGA-NPs and DBZ-NPs. (D) Measured weight of inguinal WAT. (E) Blood glucose concentration and area under curve quantification during GTT performed on the mice receiving PLGA-NPs and DBZ-NPs. (F) Blood glucose concentration and area above curve quantification during ITT performed on the mice treated with PLGA-NPs and DBZ-NPs. (G-I) Quantification of serum levels of (G) glucose, (H) cholesterol, and (I) insulin from fasting mice treated with PLGA-NPs and DBZ-NPs. Data are presented as the means ± SEM. n ≥ 4 mice for each group. *p < 0.05, **p < 0.01, N.S., non-significant.

beige adipocytes. Moreover, as several other cell types, such as immune cells and endothelial cells, reside in the WAT depot, these cells may also play an important role in regulating systemic metabolism. For example, Notch signaling has been implicated in the M1-versus-M2 macrophage specification and thereby affects inflammation and insulin resistance. To ne future question is whether DBZ-NPs induce the shift between macrophage subpopulations and

thereby contribute to metabolic benefits. Interestingly, a recent study reported that systemic delivery of DBZ, but not adipocyte-specific deletion of Rbpj, inhibited Akt phosphorylation in WATs and 3T3-L1 adipocytes and reduced glucose uptake into epididymal adipose tissues. These observations suggest a Notch-independent action of DBZ. However, systemic delivery of DBZ makes it difficult to dissect whether the observed metabolic actions are direct or indirect effects.

In addition, epididymal adipose tissues are known to be resistant to browning. Here, we showed that intracellular release of DBZ leads to remarkable browning of inguinal white adipocytes, Furthermore, we observed that delivery of DBZ-NPs into only two adipose depots resulted in systemic metabolic improvement. These results therefore argue against the possibility that DBZ would cause insulin resistance in subcutaneous inguinal adipocytes.

With the global epidemic of obesity and limited success with current pharmacotherapies, our proof-of-principle studies of the local delivery of NPs to inguinal WAT open new avenues for both the fundamental understanding of the role of browning in regulating body energy homeostasis as well as the clinical translation of the brown and beige adipocyte knowledge to treat obesity and its associated diseases. As Notch signaling is highly conserved in the animal kingdom, future studies involving human adipocytes and efficacy studies in large animals are needed for successful clinical translation of this nanotherapeutic platform. Furthermore, with the discovery of a plethora of browning factors to improve energy expenditure such as β3-adrenergic pathway agonists, 37,38 bone morphogenetic proteins (BMPs), 39,40 fibroblast growth factors (FGFs), 41-43 irisin, 44 thyroid hormones, 45,46 and natriuretic peptides, 47 development of delivery systems that are both safe and offer spatiotemporal control over the delivery is essential to translate findings to the clinic.⁴⁸ Considering the versatility of polymer chemistry, new delivery systems can be envisioned. 49,50 It may be feasible to incorporate multiple browning factors simultaneously to achieve synergistic effects. In addition, functionalization of NPs with targeting ligands may be explored to enhance biological specificity and therapeutic efficacy by increasing the interaction of NPs with adipose tissue. These strategies would require further understanding and exploitation of the adipose tissue physiology and cell-material interactions. For example, the interaction between one specific peptide CKGGRAKDC and prohibitin, a vascular marker in the adipose tissue, has been employed to facilitate NP targeting to the vasculature in the adipose tissues to promote transformation of WAT to BAT. 51,52 Specifically, Xue et al. recently developed targeted PLGA-b-PEG NPs to deliver either Peroxisome Proliferator-Activated Receptor gamma (PPAR gamma) activator rosiglitazone (Rosi) or prostaglandin E2 analog (16,16-dimethyl PGE2) to adipose tissue vasculature to stimulate WAT angiogenesis and thereby promote browning.⁵²

In summary, we demonstrate a simple local delivery approach to induce browning of WAT by harnessing NP-mediated intracellular delivery and role of Notch signaling in regulating adipocyte plasticity. These Notch-inhibitor-releasing NPs support rapid cellular internalization and inhibit Notch signaling in adipocytes. Importantly, local injection of these NPs into the inguinal WAT depots in a diet-induced obese mouse model results in localized NP retention and browning of adipocytes, consequently improving the glucose homeostasis and attenuating body-weight gain of the treated mice. Our studies not only substantiate that the local browning induced by the Notch inhibition in WAT improved energy homeostasis, but also offer

new avenues to develop a potential therapeutic strategy for clinical treatment of obesity and its associated metabolic syndrome.

MATERIALS AND METHODS

Materials

The 50:50 PLGA (inherent viscosity: 0.45–0.60 dL/g) was obtained from Boehringer Ingelheim. DBZ was purchased from Tocris Bioscience. PLGA of molecular weight of 30,000 with a terminal amine group (PLGA-NH₂) was purchased from PolySciTech. The N-hydroxysuccinimidyl ester form of cyanine 5.5 (Cy5.5-NHS) was purchased from Click Chemistry Tools. Acetone and chloroform were purchased from Fisher Scientific. All other reagents and solvents were purchased from Sigma-Aldrich.

Animals

All procedures involving mice were approved by Institutional Animal Care and Use Committee. 10-week-old male HFD-induced obese mice with the C57BL/6 background were purchased from Taconic and housed under normal conditions with free access to food and water. HFD (Research Diets #D12492, 60% fat) was used to induce and maintain obesity in the mice. Mice with an average body weight of 36 g at 14 weeks started to receive weekly NP injection into the inguinal WAT depot on each side of the body at a dosage of 1 mg/mL NPs in a volume of 200 μ L PBS. After 5 weeks, mice were euthanized by a lethal dose of carbon dioxide, followed by immediate blood collection from hearts for the assessment of serological parameters and then quick dissection of inguinal WAT, BAT, and liver for the molecular and cellular analysis.

NP Synthesis and Characterization

The NPs were prepared using a nanoprecipitation method. In brief, PLGA was dissolved in acetone with or without a predefined amount of drug compounds, including DBZ or Nile red (Fluka Analytical). This polymer/drug mixture solution was injected into the aqueous stabilizer solution using a needle under magnetic stirring. The stabilizer solution consisted of a polyvinyl alcohol (PVA, 87%-90% hydrolyzed, MW 30-70 kDa) aqueous solution. The NPs were stirred for 6 hr to allow solvent evaporation. The particle suspension was then rinsed three times by centrifugation (12,000 rpm, 4°C, 45 min) and dispersed in water by stirring for 15 min. The size and zeta potential were determined by DLS using Malvern Zetasizer. NPs were stained with 1% phosphotungstic acid solution and observed for size and morphology using a transmission electron microscope (Philips CM100) operating at 200 kV. The DBZ content in the NPs was determined by high-performance liquid chromatography (HPLC) (Thermo Fisher Scientific).

DBZ Release from NPs

The release of DBZ from NPs was examined through dialysis, followed by HPLC analysis. Specifically, 1 mL DBZ-NP solution (1 mg/mL) was transferred to a dialysis tube (MWCO: 12–14 kDa) and immersed in 40 mL PBS (pH 5.0 and 7.4) at 37°C in an orbital shaker at 100 rpm. At specific time points, 12 mL of buffer solution was removed and replaced with fresh buffer solution. The sample

was extracted with chloroform, followed by reconstitution with 1 mL of a 67% solution of acetonitrile in water for HPLC analysis.

Synthesis of Cy5.5-NPs

The conjugation of a Cy5.5-NHS ester and PLGA-NH $_2$ was performed by mixing 1.2 mg of Cy5.5-NHS ester and 33 mg of PLGA-NH $_2$ in 3 mL of DMSO in a Schlenk flask under nitrogen and stirring overnight at room temperature in darkness. After the reaction, the final product was purified by using the solvent/non-solvent technique. The reaction mixture was dropped into 40 mL of methanol cooled in ice bath and centrifuged at 8,000 rpm at 4°C for 30 min. The pellet was dissolved again in DMSO, and the washing procedure was repeated for two more cycles. The final pellet was dried using vacuum oven for 24 hr at room temperature. The conjugation of Cy5.5-NHS ester to PLGA-NH $_2$ was confirmed with a UV-vis spectrophotometer (Cary 300, Varian). The PLGA-Cy5.5 NPs were prepared following the standard protocol described above.

Isolation and Culture of the SVF Cells from Inguinal WAT

Inguinal WATs were specifically dissected out and minced into small pieces, followed by the digestion of 1.5 mg/mL collagenase in DMEM with gentle agitation at 37°C for 1.5–2 hr. The digestion was terminated by 10% (v/v) fetal bovine serum (FBS) in DMEM. Then the mixture solution was filtered with a 100- μ m cell strainer (BD Flacon) and subjected to a brief centrifugation at 450 \times g for 5 min. After removal of the floating lipid layer and supernatant, the pellet was resuspended and maintained with DMEM supplemented with 20% (v/v) FBS and 1% penicillin/streptomycin at 37°C with 5% CO₂.

Cellular Uptake of NPs

SVF cells were seeded in an 8-well chamber slide (Lab-Tek) at a density of 10,000 cells per well and cultured for 24 hr. Then cells were exposed to DMEM containing 0.1 mg/mL Nile-red-loaded PLGA NPs for 10 and 60 min. After washing twice with PBS, cells were subsequently incubated with 50 nM LTG (Life Technologies) for 30 min and 1 mg/mL Hoechst 33342 (Life Technologies) for 10 min at 37°C. Images were taken with a Leica DMI 6000B fluorescence microscope.

Ex Vivo Tissue Uptake of NPs

Inguinal WATs were freshly isolated from mice and rinsed with PBS for three times, followed by the incubation with DMEM containing 0.1 mg/mL Nile-red-loaded NPs for 24 hr. Then after removal of the NP suspension, tissues were rinsed with PBS and stained with 1 mg/mL Hoechst 33342 for 10 min, followed by the fluorescent imaging with a Leica DMI 6000B fluorescence microscope. Meanwhile, tissue uptake of NPs was also characterized by TEM. Briefly, tissue samples (1- to 2-mm blocks) were fixed in 2.5% glutaraldehyde (in 0.1 M cacodylate buffer). Samples were rinsed with 0.1 M cacodylate buffer followed by fixation in 2% osmium tetroxide for 2 hr. After washing with deionized water, samples were dehydrated in series of graded ethanol and embedded in Epon generic resin. Ultra-thin sections (90 nm) were cut and stained with uranyl acetate and lead citrate. Stained sections

were examined under CM-100 transmission electron microscope attached with Gatan imaging system.

Adipogenic Differentiation of SVF Cells with NPs

SVF cells were cultured in tissue culture plates until confluence. Before adipogenic induction, cells were rinsed with PBS for three times and incubated with DMEM containing NPs with the final concentration of 0.1 mg/mL for 1 hr. After removal of the NP suspension, cells were rinsed with PBS carefully and subjected to the adipogenic induction medium containing DMEM, 10% (v/v) FBS, 2.85 µM insulin, 0.3 µM dexamethasone, and 0.63 mM 3-isobutylmethylxanthine for 4 days. At day 5, cells were treated with NPs again with the same procedure described above, followed by the adipogenic differentiation medium containing DMEM, 200 nM insulin, and 10 nM triiodothyronine for additional 4 days until adipocytes matured.

Adipocyte OCR Measurement

Primary SVF cells from inguinal WAT of three different mice were cultured and seeded into the seahorse XF24 microplate (Seahorse Biosciences) at the density of 20,000 cells per well. Cells were induced and differentiated to mature adipocytes with the treatment of PLGA-NPs and DBZ-NPs following the protocols described above. After 8 days of differentiation, mature adipocytes were washed twice with PBS and pre-incubated in XF Base Medium supplemented with 20 mM glucose, 2 mM glutamine, and 1 mM pyruvate for 1–2 hr at 37°C in a CO₂-free environment. OCR was measured on the XF Extracellular Flux Analyzer (Seahorse Biosciences) after sequential injection of Oligomycin (1 mM), FCCP (1 mM), and Rotenone/Antimycin A (0.5 μ M). OCR values presented were normalized to protein mass.

In Vivo Imaging Studies

After anesthetization by a ketamine-xylazine cocktail, mice were injected with 1 mg/mL Cy5.5-conjugated PLGA NPs suspended in PBS in the inguinal WAT. Images were taken with the IVIS LuminalIimaging system (Caliper) at 24, 48, and 72 hr post-injection. After the 72 hr scanning, mice were euthanized, and multiple related tissues were collected, followed by the ex vivo imaging. The fluorescent images were analyzed by the Living Image Software.

Measurements of Blood Glucose

For GTT, mice were injected i.p. with 100 mg/mL D-glucose (2 g/kg body weight) after 16 hr of fasting. Blood was drawn from tails, and glucose levels were measured by a glucometer (Accu-Check Active, Roche). For ITT, mice were injected i.p. with human insulin (Santa Cruz Biotechnology) (0.75 U per kg body weight) after 4 hr of fasting. Glucose concentrations were measured in the blood drawn from tails. For both GTT and ITT, mice were separated into one per cage with random orders.

Measurement of Serological Parameters

Serum levels of free fatty acids, glucose, cholesterol, and triglycerides from fasted mice after treatment of NPs for 5 weeks were examined by standard kits from Randox Laboratories. The insulin level in the

serum was measured by ELISA according to the manufacturer's instructions (ALPCO).

H&E and Immunohistochemistry Staining

Portions of inguinal WAT were fixed in 10% formalin for 24 hr at room temperature, embedded into paraffin, and cut into 5- μm slides. Slides were deparaffinized and incubated with xylene, ethanol, and water sequentially for rehydration according to standard protocols. For H&E staining, slides were stained with hematoxylin for 15 min, followed by eosin staining for 1 min. For immunohistochemistry staining, slides were incubated in 0.01 M sodium citrate (pH 6.0) and heated at 96°C for 20 min to retrieve antigens. Ucp1 immunohistochemistry was conducted in a Dako Autostainer (Dako). Slides were stained with the Ucp1 primary antibody (ab10983, Abcam) at 1:500 dilution for overnight at 4°C. Samples were incubated with the horseradish peroxidase (HRP)-conjugated secondary antibody (ab6721) at 1:500 dilution for 1 hr at room temperature. Then 3,3'-diaminobenzidine (DAB) was used as the chromogen to visualize the labeling. Images were collected through an Aperio Scan Scope slide scanner (Aperio).

Total RNA Extraction, cDNA Synthesis, and qPCR

Total RNA was extracted from cells or tissues through Trizol (Life Technologies) in accordance with the manufacturer's protocol. After the measurement of RNA concentration by the Nanodrop (Thermo Fisher Scientific), 5 μg RNA was reverse transcribed to cDNA with random hexamer primers by M-MLV reverse transcriptase (Invitrogen). The qPCR was performed on the Roche Light Cycler 96 PCR System (Roche). The sequences of primers were listed in Table S3. For the result analysis, the $2^{-\Delta\Delta CT}$ method was used to calculate the relevant changes of gene expression after normalization to the 18S rRNA.

Protein Extraction and Western Blot Analysis

Protein was extracted from cell or tissue samples with RIPA buffer containing 50 mM Tris-HCl (pH 8.0), 150 mM NaCl, 1% Nonidet P-40, 0.5% sodium deoxycholate, and 0.1% SDS. Protein concentration was determined by Pierce BCA protein assay reagent (Pierce). Proteins were separated by SDS-PAGE and transferred to a polyvinylidene fluoride (PVDF) membrane (Millipore), followed by the blocking with 5% milk for 1 hr. Then the membranes were incubated with primary antibodies at 4°C overnight. The Hes1 (SC-166378), Pgc1- α (SC-13067), and β -actin (SC-47778) antibodies (Santa Cruz Biotechnology) were all diluted 1:1,000. The HRP-conjugated secondary antibodies (antirabbit immunoglobulin G [IgG], 7074S or anti-mouse IgG, 7076S, Cell Signaling Technology) were diluted 1:5,000. After incubation with secondary antibodies for 2 hr, the enhanced chemiluminescence western blotting substrate (Pierce Biotechnology) was used to detect signals with a ChemiDocTM Touch Imaging System (Bio-Rad).

Statistical Analysis

Quantitative data were represented as mean \pm SEM. p values were calculated by a two-tailed Student's t test. p < 0.05 was considered to be statistically significant.

SUPPLEMENTAL INFORMATION

Supplemental Information includes seven figures and three tables and can be found with this article online at http://dx.doi.org/10.1016/j.ymthe.2017.05.020.

AUTHOR CONTRIBUTIONS

C.J., M.A.C.-V., S.K., and M.D. conceived and designed research; C.J., M.A.C.-V., F.Y., L.K., N.N., G.U., and M.P.M. performed research; C.J., M.A.C.-V., F.Y., L.K., S.K., and M.D. analyzed and interpreted data; and C.J., M.A.C.-V., and M.D. wrote the paper.

CONFLICTS OF INTEREST

M.D., C.J., L.K., and S.K. are co-inventors on a patent application entitled "Polymer-based Therapeutics for Inductive Browning of Fat" (International PCT Patent Application Number: PCT/US16/58997) and disclose financial interest in Adipo Therapeutics, a biotechnology company developing polymer technologies for applications in adipocytes. The remaining authors declare no competing financial interests.

ACKNOWLEDGMENTS

We thank Donna Brooks and Gabrielle Shafer for assistance with histology and immunohistochemistry, Robert Considine and Anthony Acton for assistance with measurement of serological parameters, and Xiaoqi Liu for providing access to XF Extracellular Flux Analyser. The study is partially supported by NIH grants R01CA212609 and P30CA023168. Funding support from the Showalter Trust, NSF grant IIP-1664353, the Purdue Research Foundation, the Purdue Start-up Package, and the Transdisciplinary Obesity Prevention Research Sciences (TOPRS) Program is also greatly appreciated.

REFERENCES

- Ogden, C.L., Carroll, M.D., Kit, B.K., and Flegal, K.M. (2014). Prevalence of child-hood and adult obesity in the United States, 2011-2012. JAMA 311, 806-814.
- Colman, E., Golden, J., Roberts, M., Egan, A., Weaver, J., and Rosebraugh, C. (2012). The FDA's assessment of two drugs for chronic weight management. N. Engl. J. Med. 367, 1577–1579.
- Gautron, L., Elmquist, J.K., and Williams, K.W. (2015). Neural control of energy balance: Translating circuits to therapies. Cell 161, 133–145.
- Seale, P., and Lazar, M.A. (2009). Brown fat in humans: Turning up the heat on obesity. Diabetes 58, 1482–1484.
- van Marken Lichtenbelt, W.D., Vanhommerig, J.W., Smulders, N.M., Drossaerts, J.M., Kemerink, G.J., Bouvy, N.D., Schrauwen, P., and Teule, G.J. (2009). Cold-activated brown adipose tissue in healthy men. N. Engl. J. Med. 360, 1500–1508.
- Virtanen, K.A., Lidell, M.E., Orava, J., Heglind, M., Westergren, R., Niemi, T., Taittonen, M., Laine, J., Savisto, N.J., Enerbäck, S., and Nuutila, P. (2009). Functional brown adipose tissue in healthy adults. N. Engl. J. Med. 360, 1518–1525.
- Harms, M., and Seale, P. (2013). Brown and beige fat: Development, function and therapeutic potential. Nat. Med. 19, 1252–1263.
- Cypess, A.M., Lehman, S., Williams, G., Tal, I., Rodman, D., Goldfine, A.B., Kuo, F.C., Palmer, E.L., Tseng, Y.H., Doria, A., et al. (2009). Identification and importance of brown adipose tissue in adult humans. N. Engl. J. Med. 360, 1509–1517.
- Ohno, H., Shinoda, K., Spiegelman, B.M., and Kajimura, S. (2012). PPARγ agonists induce a white-to-brown fat conversion through stabilization of PRDM16 protein. Cell Metab. 15, 395–404.

- Seale, P., Conroe, H.M., Estall, J., Kajimura, S., Frontini, A., Ishibashi, J., Cohen, P., Cinti, S., and Spiegelman, B.M. (2011). Prdm16 determines the thermogenic program of subcutaneous white adipose tissue in mice. J. Clin. Invest. 121, 96–105.
- Rosenwald, M., Perdikari, A., Rülicke, T., and Wolfrum, C. (2013). Bi-directional interconversion of brite and white adipocytes. Nat. Cell Biol. 15, 659–667.
- Ye, L., Wu, J., Cohen, P., Kazak, L., Khandekar, M.J., Jedrychowski, M.P., Zeng, X., Gygi, S.P., and Spiegelman, B.M. (2013). Fat cells directly sense temperature to activate thermogenesis. Proc. Natl. Acad. Sci. USA 110, 12480–12485.
- Cao, L., Choi, E.Y., Liu, X., Martin, A., Wang, C., Xu, X., and During, M.J. (2011).
 White to brown fat phenotypic switch induced by genetic and environmental activation of a hypothalamic-adipocyte axis. Cell Metab. 14, 324–338.
- Shabalina, I.G., Petrovic, N., de Jong, J.M., Kalinovich, A.V., Cannon, B., and Nedergaard, J. (2013). UCP1 in brite/beige adipose tissue mitochondria is functionally thermogenic. Cell Rep. 5, 1196–1203.
- Pfannenberg, C., Werner, M.K., Ripkens, S., Stef, I., Deckert, A., Schmadl, M., Reimold, M., Häring, H.U., Claussen, C.D., and Stefan, N. (2010). Impact of age on the relationships of brown adipose tissue with sex and adiposity in humans. Diabetes 59, 1789–1793.
- 16. Ouellet, V., Routhier-Labadie, A., Bellemare, W., Lakhal-Chaieb, L., Turcotte, E., Carpentier, A.C., and Richard, D. (2011). Outdoor temperature, age, sex, body mass index, and diabetic status determine the prevalence, mass, and glucose-uptake activity of 18F-FDG-detected BAT in humans. J. Clin. Endocrinol. Metab. 96, 192–199.
- Bi, P., and Kuang, S. (2015). Notch signaling as a novel regulator of metabolism. Trends Endocrinol. Metab. 26, 248–255.
- Bi, P., Shan, T., Liu, W., Yue, F., Yang, X., Liang, X.R., Wang, J., Li, J., Carlesso, N., Liu, X., and Kuang, S. (2014). Inhibition of Notch signaling promotes browning of white adipose tissue and ameliorates obesity. Nat. Med. 20, 911–918.
- Pajvani, U.B., Qiang, L., Kangsamaksin, T., Kitajewski, J., Ginsberg, H.N., and Accili, D. (2013). Inhibition of Notch uncouples Akt activation from hepatic lipid accumulation by decreasing mTorc1 stability. Nat. Med. 19, 1054–1060.
- Kamaly, N., Yameen, B., Wu, J., and Farokhzad, O.C. (2016). Degradable controlledrelease polymers and polymeric nanoparticles: Mechanisms of controlling drug release. Chem. Rev. 116, 2602–2663.
- Vitali, A., Murano, I., Zingaretti, M.C., Frontini, A., Ricquier, D., and Cinti, S. (2012).
 The adipose organ of obesity-prone C57BL/6J mice is composed of mixed white and brown adipocytes. J. Lipid Res. 53, 619–629.
- Lin, S., Shen, H., Jin, B., Gu, Y., Chen, Z., Cao, C., Hu, C., Keller, C., Pear, W.S., and Wu, L. (2013). Brief report: Blockade of Notch signaling in muscle stem cells causes muscular dystrophic phenotype and impaired muscle regeneration. Stem Cells 31, 823–828.
- Wen, Y., Bi, P., Liu, W., Asakura, A., Keller, C., and Kuang, S. (2012). Constitutive Notch activation upregulates Pax7 and promotes the self-renewal of skeletal muscle satellite cells. Mol. Cell. Biol. 32, 2300–2311.
- Liu, P., Ping, Y., Ma, M., Zhang, D., Liu, C., Zaidi, S., Gao, S., Ji, Y., Lou, F., Yu, F., et al. (2016). Anabolic actions of Notch on mature bone. Proc. Natl. Acad. Sci. USA 113, F2152-F2161
- Chen, L., Holmstrøm, K., Qiu, W., Ditzel, N., Shi, K., Hokland, L., and Kassem, M. (2014). MicroRNA-34a inhibits osteoblast differentiation and in vivo bone formation of human stromal stem cells. Stem Cells 32, 902–912.
- Noguera-Troise, I., Daly, C., Papadopoulos, N.J., Coetzee, S., Boland, P., Gale, N.W., Lin, H.C., Yancopoulos, G.D., and Thurston, G. (2006). Blockade of Dll4 inhibits tumour growth by promoting non-productive angiogenesis. Nature 444, 1032–1037.
- Benedito, R., Roca, C., Sörensen, I., Adams, S., Gossler, A., Fruttiger, M., and Adams, R.H. (2009). The notch ligands Dll4 and Jagged1 have opposing effects on angiogenesis. Cell 137, 1124–1135.
- Jiang, C., Kuang, L., Merkel, M.P., Yue, F., Cano-Vega, M.A., Narayanan, N., Kuang, S., and Deng, M. (2015). Biodegradable polymeric microsphere-based drug delivery for inductive browning of fat. Front. Endocrinol. (Lausanne) 6, 169.
- Mitragotri, S., Burke, P.A., and Langer, R. (2014). Overcoming the challenges in administering biopharmaceuticals: Formulation and delivery strategies. Nat. Rev. Drug Discov. 13, 655–672.

- Conner, S.D., and Schmid, S.L. (2003). Regulated portals of entry into the cell. Nature 422, 37–44.
- Panyam, J., Zhou, W.Z., Prabha, S., Sahoo, S.K., and Labhasetwar, V. (2002). Rapid endo-lysosomal escape of poly(DL-lactide-co-glycolide) nanoparticles: Implications for drug and gene delivery. FASEB J. 16, 1217–1226.
- Pajvani, U.B., Shawber, C.J., Samuel, V.T., Birkenfeld, A.L., Shulman, G.I., Kitajewski, J., and Accili, D. (2011). Inhibition of Notch signaling ameliorates insulin resistance in a FoxO1-dependent manner. Nat. Med. 17, 961–967.
- 33. Stanford, K.I., Middelbeek, R.J., Townsend, K.L., An, D., Nygaard, E.B., Hitchcox, K.M., Markan, K.R., Nakano, K., Hirshman, M.F., Tseng, Y.H., and Goodyear, L.J. (2013). Brown adipose tissue regulates glucose homeostasis and insulin sensitivity. J. Clin. Invest. 123, 215–223.
- 34. Stanford, K.I., Middelbeek, R.J., Townsend, K.L., Lee, M.Y., Takahashi, H., So, K., Hitchcox, K.M., Markan, K.R., Hellbach, K., Hirshman, M.F., et al. (2015). A novel role for subcutaneous adipose tissue in exercise-induced improvements in glucose homeostasis. Diabetes 64, 2002–2014.
- Xu, H., Zhu, J., Smith, S., Foldi, J., Zhao, B., Chung, A.Y., Outtz, H., Kitajewski, J., Shi, C., Weber, S., et al. (2012). Notch-RBP-J signaling regulates the transcription factor IRF8 to promote inflammatory macrophage polarization. Nat. Immunol. 13, 642–650.
- Sparling, D.P., Yu, J., Kim, K., Zhu, C., Brachs, S., Birkenfeld, A.L., and Pajvani, U.B. (2015). Adipocyte-specific blockade of gamma-secretase, but not inhibition of Notch activity, reduces adipose insulin sensitivity. Mol. Metab. 5, 113–121.
- Himms-Hagen, J., Melnyk, A., Zingaretti, M.C., Ceresi, E., Barbatelli, G., and Cinti, S. (2000). Multilocular fat cells in WAT of CL-316243-treated rats derive directly from white adipocytes. Am. J. Physiol. Cell Physiol. 279, C670–C681.
- Nguyen, K.D., Qiu, Y., Cui, X., Goh, Y.P., Mwangi, J., David, T., Mukundan, L., Brombacher, F., Locksley, R.M., and Chawla, A. (2011). Alternatively activated macrophages produce catecholamines to sustain adaptive thermogenesis. Nature 480, 104–108.
- Tseng, Y.H., Kokkotou, E., Schulz, T.J., Huang, T.L., Winnay, J.N., Taniguchi, C.M., Tran, T.T., Suzuki, R., Espinoza, D.O., Yamamoto, Y., et al. (2008). New role of bone morphogenetic protein 7 in brown adipogenesis and energy expenditure. Nature 454, 1000–1004.
- Whittle, A.J., Carobbio, S., Martins, L., Slawik, M., Hondares, E., Vázquez, M.J., Morgan, D., Csikasz, R.I., Gallego, R., Rodriguez-Cuenca, S., et al. (2012). BMP8B increases brown adipose tissue thermogenesis through both central and peripheral actions. Cell 149, 871–885.
- 41. Jonker, J.W., Suh, J.M., Atkins, A.R., Ahmadian, M., Li, P., Whyte, J., He, M., Juguilon, H., Yin, Y.Q., Phillips, C.T., et al. (2012). A PPARγ-FGF1 axis is required for adaptive adipose remodelling and metabolic homeostasis. Nature 485, 391–394.
- Fisher, F.M., Kleiner, S., Douris, N., Fox, E.C., Mepani, R.J., Verdeguer, F., Wu, J., Kharitonenkov, A., Flier, J.S., Maratos-Flier, E., and Spiegelman, B.M. (2012).
 FGF21 regulates PGC-1α and browning of white adipose tissues in adaptive thermogenesis. Genes Dev. 26, 271–281.
- Fu, L., John, L.M., Adams, S.H., Yu, X.X., Tomlinson, E., Renz, M., Williams, P.M., Soriano, R., Corpuz, R., Moffat, B., et al. (2004). Fibroblast growth factor 19 increases metabolic rate and reverses dietary and leptin-deficient diabetes. Endocrinology 145, 2594–2603
- 44. Boström, P., Wu, J., Jedrychowski, M.P., Korde, A., Ye, L., Lo, J.C., Rasbach, K.A., Boström, E.A., Choi, J.H., Long, J.Z., et al. (2012). A PGC1-α-dependent myokine that drives brown-fat-like development of white fat and thermogenesis. Nature 481, 463–468.
- Lin, J.Z., Martagón, A.J., Cimini, S.L., Gonzalez, D.D., Tinkey, D.W., Biter, A., Baxter, J.D., Webb, P., Gustafsson, J.Å., Hartig, S.M., and Phillips, K.J. (2015). Pharmacological Activation of Thyroid Hormone Receptors Elicits a Functional Conversion of White to Brown Fat. Cell Rep. 13, 1528–1537.
- Silva, J.E. (2006). Thermogenic mechanisms and their hormonal regulation. Physiol. Rev. 86, 435–464.
- 47. Bordicchia, M., Liu, D., Amri, E.Z., Ailhaud, G., Dessi-Fulgheri, P., Zhang, C., Takahashi, N., Sarzani, R., and Collins, S. (2012). Cardiac natriuretic peptides act via p38 MAPK to induce the brown fat thermogenic program in mouse and human adipocytes. J. Clin. Invest. 122, 1022–1036.

- 48. Wei, W., Dutchak, P.A., Wang, X., Ding, X., Wang, X., Bookout, A.L., Goetz, R., Mohammadi, M., Gerard, R.D., Dechow, P.C., et al. (2012). Fibroblast growth factor 21 promotes bone loss by potentiating the effects of peroxisome proliferator-activated receptor γ. Proc. Natl. Acad. Sci. USA 109, 3143–3148.
- Deng, M., Kumbar, S.G., Wan, Y.Q., Toti, U.S., Allcock, H.R., and Laurencin, C.T. (2010). Polyphosphazene polymers for tissue engineering: An analysis of material synthesis, characterization and applications. Soft Matter 6, 3119–3132.
- Deng, M., Nair, L.S., Nukavarapu, S.P., Kumbar, S.G., Jiang, T., Weikel, A.L., Krogman, N.R., Allcock, H.R., and Laurencin, C.T. (2010). In situ porous structures:
- A unique polymer erosion mechanism in biodegradable dipeptide-based polyphosphazene and polyester blends producing matrices for regenerative engineering. Adv. Funct. Mater. 20, 2743–2957.
- Kolonin, M.G., Saha, P.K., Chan, L., Pasqualini, R., and Arap, W. (2004). Reversal of obesity by targeted ablation of adipose tissue. Nat. Med. 10, 625–632.
- Xue, Y., Xu, X., Zhang, X.Q., Farokhzad, O.C., and Langer, R. (2016). Preventing dietinduced obesity in mice by adipose tissue transformation and angiogenesis using targeted nanoparticles. Proc. Natl. Acad. Sci. USA 113, 5552–5557.